ELSEVIER

Sensors and Actuators A 92 (2001) 60–66

SENSORS AND ACTUATORS A PHYSICAL

www.elsevier.com/locate/sna

New p–i–n Si:H imager configuration for spatial resolution improvement

Manuela Vieira[a,*], Miguel Fernandes[a], João Martins[a], Paula Louro Antunes[a], António Maçarico[a], Reinhard Schwarz[a], Markus B. Schubert[b]

[a]*Electronics and Communications Department, ISEL, R. Conselheiro Emídio Navarro, P 1949-014 Lisboa, Portugal*
[b]*Institut fur Physikalische Elektronik, Universitat Stuttgart, Pfaffenwaldring 47, D-70569 Stuttgart, Germany*

Accepted 20 December 2000

Abstract

Amorphous glass/ZnO:Al/p(a-Si:H)/i(a-Si:H)/n(a-$Si_{1-x}C_x$:H)/Al imagers with different n-layer resistivities were produced by plasma enhanced chemical vapour deposition technique (PE-CVD). An image is projected onto the sensing element and leads to spatially confined depletion regions that can be readout by scanning the photodiode with a low-power modulated laser beam. The essence of the scheme is the analog readout, and the absence of semiconductor arrays or electrode potential manipulations to transfer the information coming from the transducer.

The influence of the intensity of the optical image projected onto the sensor surface is correlated with the sensor output characteristics (sensitivity, linearity, blooming, resolution and signal-to-noise ratio) are analysed for different material compositions ($0.5 < x < 1$). The results show that the responsivity and the spatial resolution are limited by the conductivity of the doped layers. An enhancement of one order of magnitude in the image intensity signal and on the spatial resolution are achieved at 0.2 mW cm^{-2} light flux by decreasing the n-layer conductivity by the same amount.

A physical model supported by electrical simulation gives insight into the image-sensing technique used. © 2001 Elsevier Science B.V. All rights reserved.

Keywords: Solid state transducer; a-Si:H p–i–n devices; Optical sensors; Imager; Image acquisition and representation; Analog readout

1. Introduction

When we try to capture and analyse light, we enter the realm of detectors and imaging technologies. Whether we want to view images or count photons, we use devices that work by absorbing photons and turning them into information. Three forces direct the evolution of the image sensors: advances in technology determine what is possible, algorithms determine what is practical, and applications determine what is desirable. If we wanted to generalise about areas in which detectors and imaging technology can improve, we could talk about collecting information more quickly and efficiently, at more wavelengths, with more compact and user-friendly devices or interfaces.

Any conventional solid state imaging device consists of an array of sensing elements combined with some form of transport mechanism to deliver these sensor outputs to the periphery of the device. Sensors used in commercial devices include photodiode arrays, complementary metal oxide semiconductors, charge injecting devices, and bipolar transistors. All of these devices use essentially the same light-sensing mechanism. Photons penetrating a depletion region generate electron–hole pairs. These carriers are swept away by the electric field across the depletion region and generate a small transverse photocurrent.

If the illumination is not uniform, different packets of charges are accumulated beneath the dark and the illuminated regions. This spatial distribution is responsible by an electric field modulation across the depletion region [1–3] that can be sensed if a small-signal scanning beam is used to readout the photo-generated carriers. Based on this effect, microcrystalline [4,5] and amorphous [6] optical TCO/p–i–n/metal image transducers were developed. Those sensors are different from charge-coupled devices (CCD) [7]. In that no special photolithography techniques for patterning the optical sensor array or voltage requirements to transfer the information are needed. A single photodiode as sensing element and a modulated low-power beam of laser light to ''paint'' the image directly is what is needed to restore an image.

* Corresponding author. Tel.: +351-1-8317181; fax: +351-1-8317114.
E-mail address: mv@isel.pt (M. Vieira).

0924-4247/01/$ – see front matter © 2001 Elsevier Science B.V. All rights reserved.
PII: S0924-4247(01)00540-4

In order to clarify what limits the image resolution modifications on the transducer structure are proposed and discussed. Hydrogenated amorphous silicon n-layers with different doping levels were deposited on a ZnO:Al/p/i structure and a thin metal layer was evaporated on them. The effect of the sensor structure (contact geometry, n-layer conductivity) and image brightness on the output characteristics is discussed. A model for the transducer operation supported by an electrical circuit simulation is presented.

2. Operation principle and electrical modelling

2.1. Image representation

Under non-uniform steady illumination, different packets of charges are accumulated beneath the dark and the illuminated regions [1–3]. This anisotropic spatial distribution is responsible for an electric field modulation across the depletion region and for a shrinking of the depletion region at the illuminated regions. If, in addition, a weak light spot is scanning the device, the carriers that are generated by the probe beam in the dark regions are separated by the junction electric field and collected (high ac component of the current, low $X_{m,n}$ values). Those generated at the illuminated region, inside the depletion region, drift in the lateral direction due to the local lowering of the potential barrier and recombine, or are trapped inside the amorphous bulk (low ac component of the current, high $X_{m,n}$ values).

2.2. Electrical model and simulation

Based on the above model, the p–i–n image sensor was modelled as an array of photodiodes interconnected through lateral resistors [8]. Fig. 1 depicts the electrical model for explaining the sensing methodology, in addition the sensor configuration and the depletion regions (dotted lines) are visualised. On the right side, a fraction of the electrical circuit, being part of the non-planar structure used for future simulation is presented. Each photodiode (D) was replaced by its incremental resistance (r_d), and connected to its four neighbours, in a row-line matrix, by the resistors R_{Ln} and R_{Lp} that model the sheet resistance of the n- and p-doped layers, respectively. The contacts establish the points for transversal measurements (V) and the scanner is simulated through a sine-wave current source (0.1 mA, 10 Hz) applied from each top node of the circuit to the *ground*. Those nodes are the diode anodes, i.e. the $m \times n$ points used for voltage readout obtained using a SPICE-based simulator [10].

Several parameters such as contact geometry, layer resistivity, and image brightness can be modelled. The contact shaping is simulated by choosing the points for voltage readout (V and the *ground*). If strip contacts are used, those points are fixed at circuit nodes where R_L are short-circuited (the contact regions). If the contacts cover the entire surface, they change for each $m \times n$ value readout, as is shown in Fig. 1. The conductivity of the doped layers is modelled by changing R_L for the whole circuit accordingly (higher conductivities correspond to lower values of R_L). The brightness of the images is obtained by changing r_d on the points allocated to the image area.

The simulation procedure has two main phases: the circuit construction and the simulation process. In the first phase, the input parameters and the array dimensions are defined in order to include the image area, the surrounding dark region, and the contacts. In the second phase, a voltage distribution composed of a matrix of $m \times n$ values is obtained. Each simulation run corresponds to a different assigned node where the scanner source is applied. The stored values are the amplitudes of the sinusoidal small signals taken in each simulation process step. The image-intensity matrix is obtained as described in Section 3.2.

3. Experimental

3.1. Device deposition and characterisation

A series of large area (3 cm × 3 cm) single layers and image transducers in the assembly glass/ZnO:Al/p(Si:H)/

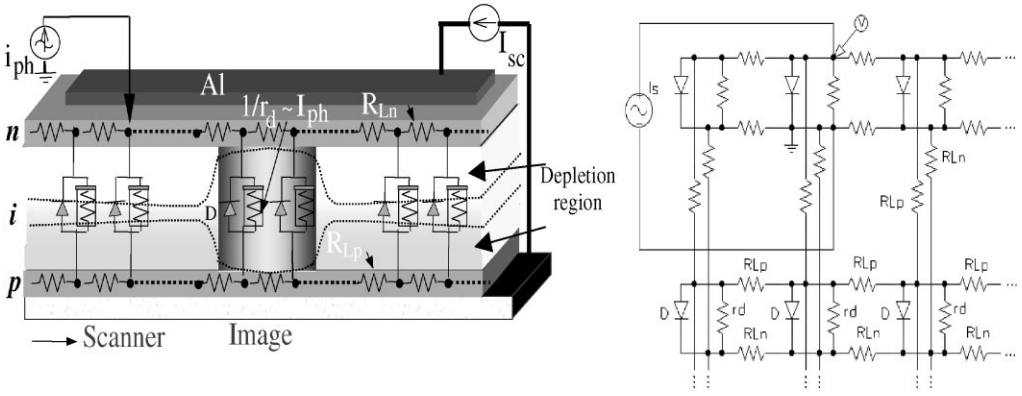

Fig. 1. Electrical model, sensor configuration and the depletion regions (dotted lines). Insert: a fraction of the electrical circuit used for simulation is depicted.

i(Si:H)/n(Si_xC_{1-x}:H)/Al were produced. The p–i–n Si:H junction acts as a sensing element, the back and the front contacts are used as electrical interfaces.

All the layers in p–i–n transducers were deposited by plasma enhanced chemical vapour deposition (PE-CVD) at a 13.56 MHz radio frequency and the contacts produced by sputtering technique [9]. The deposition pressure was 200 mTorr, the substrate temperature was held at 150°C, and the rf-power was 4 W. The deposition conditions of all the p- and i-layers were kept constant while varied in the n-layer (1–10 sccm PH_3/10 sccm SiH_4/0–20 sccm CH_4). A preliminary electrical and optical characterisation of the films was carried out by measuring the electrical conductivity in the coplanar direction and by obtaining the absorption spectra from transmission and reflection measurements. The deposited n-layers present conductivity, s_d, in the range of 1.0×10^{-5}–$2.6 \times 10^{-4}\ \Omega^{-1}\,cm^{-1}$ and optical gaps, E_{op}, between 1.8 and 2.1 eV, while for the p-type film $7 \times 10^{-5}\ \Omega^{-1}\,cm^{-1}$ and 1.8 eV were inferred. The i-layer has a dark conductivity of approximately $1 \times 10^{-10}\ \Omega^{-1}\,cm^{-1}$ and a photosensitivity higher than 10^4 under AM1.5 (100 mW cm^{-2}). The thicknesses of the p-, i- and n-layers in the transducer were 500, 5000 and 500 Å, respectively. The front contact ZnO:Al is a 300 nm thick and has a transmission of approximately 80% from 425 to 700 nm and a resistivity around $9 \times 10^{-4}\ \Omega$ cm. Two back-contact geometries were evaporated: strip contacts around the borders and large area contacts covering the entire active surface.

The transducers were characterised by current–voltage (I–V) in dark and under illumination and spectral response measurements. Open circuit voltages, V_{OC}, of the order of 0.8 V and short-circuit currents, I_{SC}, of about 8 mA cm^{-2} were measured. The devices present a good detection in the visible range (450–750 nm) with a maximum at wavelengths of the order of 600 nm.

3.2. Device operation

A focused image is projected onto the photosensitive surface through the transparent contact. For image acquisition, a low-power chopped laser spot scans the sensor in the frame mode. The readout of the injected carriers is achieved by measuring the ac component of the short-circuit current, I_{SC}. The entire process is controlled by a microcomputer which stores the currents as a two-dimensional array of discrete values, $I_{m,n}$, each one representing the photocurrent induced by the chopped light at the selected position. A $m \times n$ grid with $200\,\mu m \times 250\,\mu m$ spacing in x and y directions is used for image representation. The image intensity, $X_{m,n}$, is obtained by subtracting the input matrix $I_{m,n}$ (with image) from the background, $b_{m,n}$ (without image) and inverting the results. The signal-to-noise ratio (S/N) depends on the relationship between the light source fluxes of the scanner (Φ_S), and the image (Φ_L) for a constant value of the n-layer conductivity.

4. Results and discussion

4.1. Contact geometry versus lateral photoeffect

The contact geometry is an important parameter to define accurately the image. Several contact geometry configurations were analysed and helped to define the actual geometry [10].

Fig. 2 shows the simulated image intensity and the grey level image representation of a rectangle (3:4) using: strip contacts around the border (a) and large area contact covering the active surface (b). The values of r_d, R_{Ln} and R_{Lp} were kept constant during the simulation process, and $r_d/R_{Ln} = 10^{-2}$. The results show that contact area and location play an important role in image representation, since its location influences the carrier path before collection. As the contact area increases from the border strips to cover contacts, a decrease on the blurring effect is detected. In the configuration with border strips, the carriers after generation are diverted in the lateral direction, across $R_{Ln,p}$, towards the contact [1] decreasing the ac component of the photocurrent mainly near the image border and giving rise to a blurring effect as shown in Fig. 2a. However, if the contact area extends all over the active surface, the lateral path is short-circuited and the carriers are collected at the generated points. The image intensity increases and the blurring effect is minimised. Large area contacts all over the active surface will be used for further results.

4.2. Doped-layer resistivity versus spatial resolution

In Fig. 3, the image intensity of a circle of 6 mm diameter cut into two halves by a 2 mm gap is displayed for two transducers having different n-layer conductivities: (a) $2.6 \times 10^{-4}\ \Omega^{-1}\,cm^{-1}$ (#M006291), and (b) $1.0 \times 10^{-5}\ \Omega^{-1}\,cm^{-1}$ (#M006301). At the bottom, the corresponding simulated intensities for $r_d/R_{Ln} = 10^{-1}$ (a) and $r_d/R_{Ln} = 10^{-2}$ are shown, keeping $r_d/R_{Lp} = 10^{-2}$.

The simulated and experimental results are in good agreement. By using a low-conductivity n-layer, a good image representation is achieved (Fig. 3b), with sharp edges and almost no blur. If the n-layer conductivity is higher (Fig. 3a), the S/N decreases, the image intensity decreases and spreads out in the lateral direction. In this case, some restoring algorithms should be used to filter the noise and to sharpen the edges in blurred images [5]. Results show that the image intensity and the spatial resolution increase by one order of magnitude by decreasing the n-layer conductivity by the same amount. S/N is of the order of 32 dB for $\Phi_S/\Phi_L = 1/20$.

The observed difference in both images depends on n-layer resistivity (R_{Ln}) for a constant value of the p-layer resistivity (R_{Lp}) and light flux intensity (r_d). Due to the lateral photoeffect, under steady state illumination, the carriers tend to drift in the lateral direction across the doped layers towards the nearby dark regions. As the doped-layer conductivity increases, the ratio between the lateral and

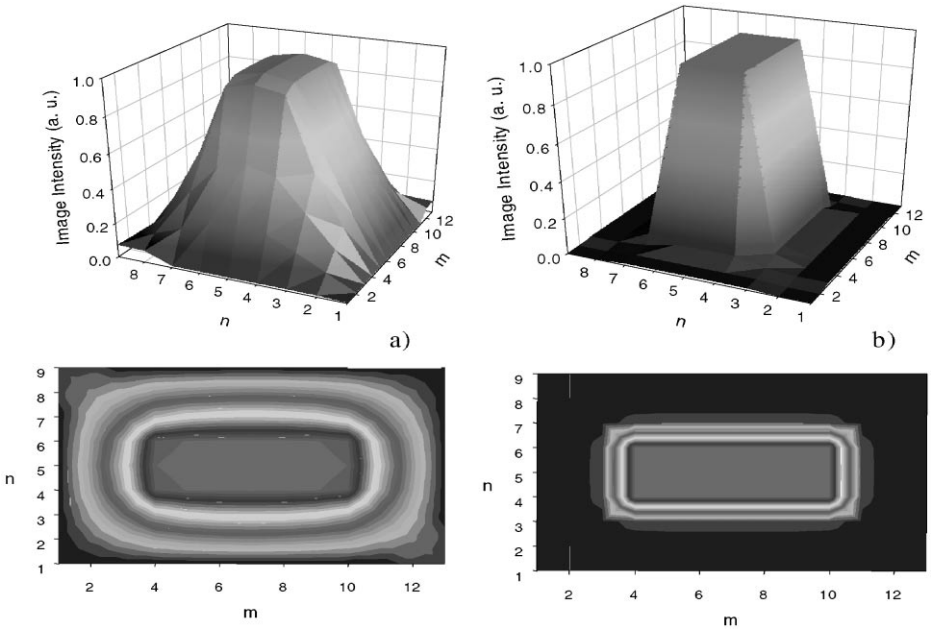

Fig. 2. Simulated image intensity of a rectangle using: (a) strip contacts; (b) a large area contact. The values of r_d, R_{Ln} and R_{Lp} were kept constant, with $r_d/R_{Ln} = 10^{-2}$. The grey level image representation and sensor configuration are also depicted.

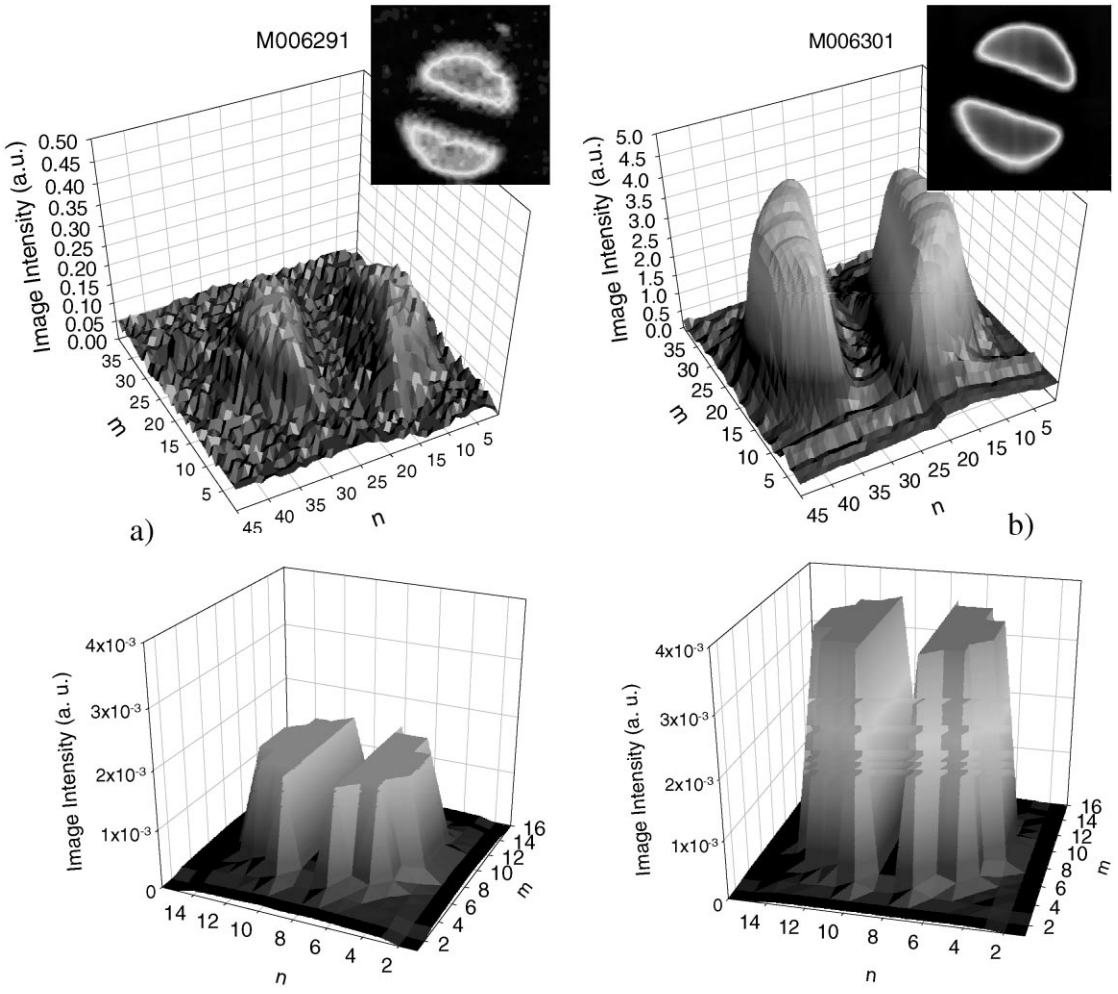

Fig. 3. Experimental (top) and simulated (bottom) image intensity and grey level representation of a circle of 6 mm diameter cut into two halves by a 2 mm gap obtained at different n-layer conductivities: (a) $2.6 \times 10^{-4}\ \Omega^{-1}\ \mathrm{cm}^{-1}$ ($r_d/R_{Ln} = 10^{-1}$); (b) $1.0 \times 10^{-5}\ \Omega^{-1}\ \mathrm{cm}^{-1}$ ($r_d/R_{Ln} = 10^{-2}$).

transverse electrical field increases decreasing the depletion layer modulation across the junction. When the conductivity of the doped layers is high, some carriers generated by the scanner inside the depletion regions drift along the doped layers towards the illuminated region (lower potential barriers/higher r_d) and are not collected, decreasing the image intensity and giving rise to some blur. Decreasing the n-layer conductivity, the lateral photoeffect is minimised. The carriers flow in the transverse direction and are collected or recombine beneath the generation point, increasing the spatial resolution.

4.3. Responsivity and linearity

In Fig. 4, the image intensity as a function of light source flux is displayed. The scanner intensity was kept constant, while the light source flux used for mapping the image into the sensor was changed (10^{-2} mW cm^{-2} < Φ_L < 6 mW cm^{-2}). As Φ_L increases, the image intensity increases, reaching its saturation value at $\Phi_L > 4$ mW cm^{-2}. The minimum illumination at which the sensor can still operate is of the order of 0.2 mW cm^{-2}. The sensor presents a good linearity at low signal levels and starts to saturate at around 70% of maximum value.

As Φ_L increases, the depletion region shrinks, initially in a linear way reaching its minimum value when the flat-band

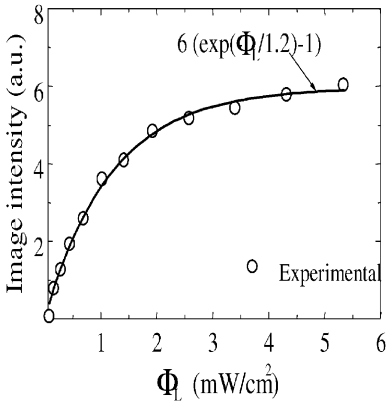

Fig. 4. Image intensity as a function of Φ_L.

condition is achieved. During the image acquisition process, only the carriers generated by the scanner within the depletion region are swept away by the existing electric field and collected (low ac component of the current, high $X_{m,n}$ values) otherwise they diffuse, recombine or are trapped in the bulk (high ac component of the current, low $X_{m,n}$ values). The image intensity will increase with Φ_L and saturates for the minimum value of the depletion width. The saturation of the image intensity is then limited by the capacity of the depletion region to hold and to separate the photocarriers

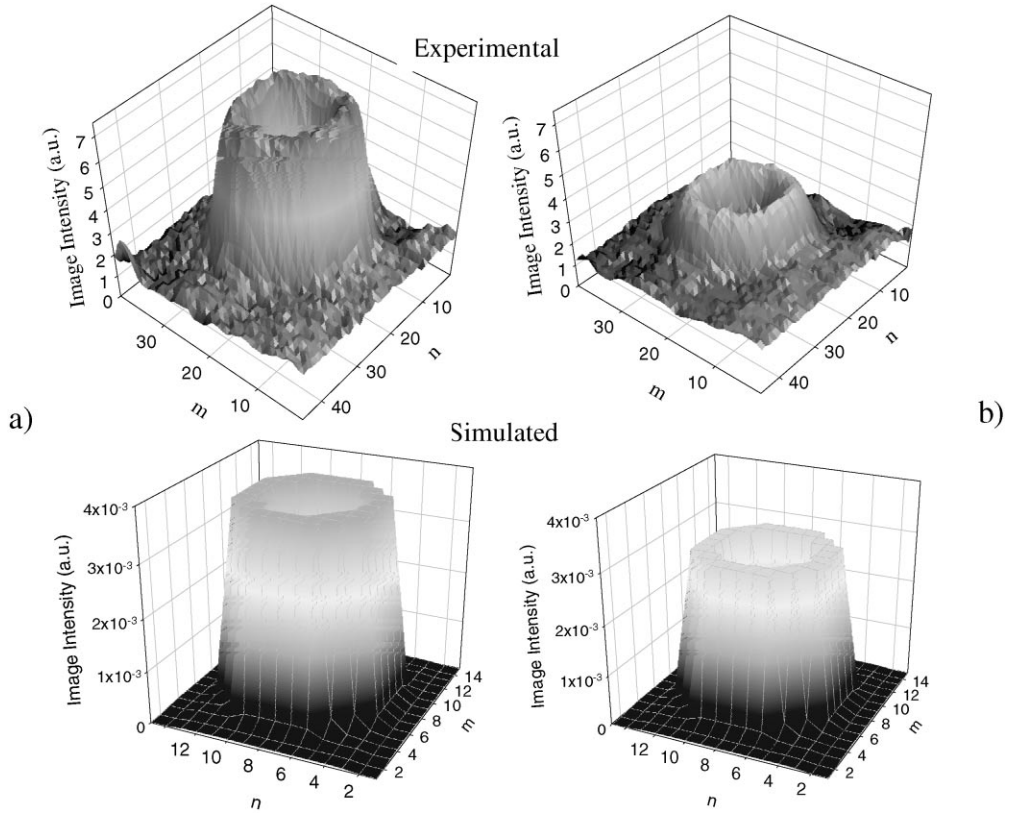

Fig. 5. Experimental (top) and simulated (bottom) image intensity representation for a 7.5 mm donut with a 2.5 mm inner hole with $\Phi_S = 2.5 \times 10^{-2}$ mW cm^{-2} and (a) $\Phi_L = 5$ mW cm^{-2}, $r_d/R_{Ln} = 10^{-2}$, (b) $\Phi_L = 0.5$ mW cm^{-2}, $r_d/R_{Ln} = 10^{-1}$.

generated by the scanner, and depends on Φ_L and on the junction electric field strength. A 7.5 mm donut having an inner hole of 2.5 mm diameter was projected onto the sensor having the most resistive n-layer (#M006301). Fig. 5a and b display the acquired images, respectively, at $\Phi_L = 5$ and 0.5 mW cm^{-2}, keeping $\Phi_S = 2.5 \times 10^{-2}$ mW cm^{-2}. For comparison at the bottom the outputs from the sensor obtained under a donut illumination for two different values of $r_d/R_{Ln} = 10^{-2}$ (a) and $r_d/R_{Ln} = 10^{-1}$ (b) are shown. R_{Ln} and R_{Lp} were kept constant during the simulation process.

The results show a good contrast between the illuminated (high $X_{m,n}$ values, low r_d values) and the dark regions (low $X_{m,n}$ values, high r_d values) even at low flux. As Φ_L increases (r_d decreases), the image intensity increases. Under full contact collection and for high resistive n-layers, the carriers injected by the scanner (ac current source) flow mainly in the transversal direction. Nevertheless, if the light source flux is high enough (saturation condition), the excess charge carriers generated from the bright part of the image spread out giving rise to some blooming at the edges (Fig. 5a).

5. Conclusions and future trends

A new semiconductor device concept has been devised which shows promise of having wide applications in optics. The image projected onto the active surface leads to spatially confined depletion regions that can be readout by scanning the photodiode with a modulated laser beam. The essence of the scheme is the analog readout, and the absence of semiconductor arrays or electrode potential manipulations to transfer the information coming from the transducer. Examples of possible applications are as imaging device, as display device, and for character recognition or facsimile.

In Fig. 6, we display the black and white image of a text word (ISEL) and a greyscale photo-representation obtained with the transducer #M006301. No image processing algorithms were used. A good resolution was obtained, although some geometrical distortion occurs due to the mechanical apparatus and the optical system used [8].

An optical ZnO:Al/a-p–i–n Si_xC_{1-x}:H/Al imager that uses a small-signal scanning beam to readout the photo-generated carriers was presented. The results show that under full contact collection, the responsivity, the linearity and the resolution are limited by the contact geometry, by the conductivity of the doped layers and by the light flux used to map the image onto the sensor. An enhancement of one order of magnitude in the image intensity and on the spatial resolution are achieved with a responsivity of 0.2 mW cm^{-2} by decreasing the n-layer conductivity by the same amount.

An optimisation of the mechanical parts and of the optical system, and more elaborate processing algorithms is still necessary for further improvement of the sensor performance.

Fig. 6. Images obtained using an amorphous p–i–n image transducer.

Acknowledgements

We would like to thank Fernando Sousa and Arnaldo Abrantes for helpful discussions concerning image processing. This work has been financially supported by PRAXIS/P/EEI/12183/1998.

References

[1] J.T. Wallmark, A new semiconductor photocell using lateral photoeffect, Proc. IRE 43 (1956) 474–483.
[2] E. Fortunato, M. Vieira, G. Lavareda, L. Ferreira, R. Martins, Material properties project design and performances of single and dual a-Si:H large area position sensitive detectors, J. Non-Cryst. Solids 164–166 (1993) 780–797.
[3] M. Vieira, Speed photodetectors based on amorphous and microcrystaliine silicon p–i–n devices, Appl. Phys. Lett. 70 (1997) 220–222.
[4] M. Vieira, A. Fantoni, S. Koynov, R. Schwarz, Microcrystalline silicon thin films for optical applications, Vacuum 52 (1999) 121–125.
[5] F. Sousa, J. Martins, M. Fernandes, A. Maçarico, R. Schwarz, M. Vieira, Image processing in a μc p–i–n image transducer, J. Non-Cryst. Solids 1228 (2000) 266–269.
[6] M. Vieira, M. Fernandes, J. Martins, P. Louro, A. Maçarico, R. Schwarz, M. Schubert, Improved resolution in a p–i–n image sensor by changing the structure of the doped layers, Mater. Res. Soc. Symp. Proc., Vol. 609 (2000) Materials Research Society.
[7] G.F. Amelio, Charge couple devices, Scientific Am. 230 (1974) 22–31.
[8] M. Vieira, E. Morgado, A. Maçarico, S. Koynov, R. Schwarz, Microcrystalline silicon thin films for optical applications, Vacuum 52 (1999) 67–71.
[9] C. Koch, M. Ito, M. Schubert, J.H. Werner, A low temperature deposition of amorphous silicon based solar cells, Mater. Res. Soc. Symp. Proc. 557 (1999) 749–754.
[10] J. Martins, F. Sousa, M. Fernandes, P. Louro, A. Maçarico, M. Vieira, The contact geometry in a 2D μc-Si:H p–i–n imager, Mater. Sci. Eng. B 69/70 (2000) 494–499.

Biographies

Manuela Vieira was born in Lisbon, Portugal, in 1951. She graduated in physics from the Faculty of Science of the University of Lisbon in 1974. In 1986, received the Master of Science in Solid State Physics, Microelectronics from the New University of Lisbon. At that time, she became Auxiliary Professor of Semiconductor and Microelectronics in ISEL, Lisbon, where she is now Coordinator Professor in semiconductor/electronics and President of the Department of Electronics and Communications. In 1984, she became member of Center of Excellence for

Microelectronics and Optoelectronics Processes-UNINOVA, Portugal. In 1993, she received the PhD in Semiconductor Materials from the New University of Lisbon. Currently, she is the head of the Group in Applied Research in Microelectronic Optoelectronic and Sensors-GIAMOS/ISEL in Lisbon, Portugal. Dr. M. Vieira has several scientific papers and more than 12 years of experience in the field of thin films and devices, her research activities have been mainly related to the transient analysis and characterisation of the transport properties of the semiconductor materials and device characterisation.

Miguel Fernandes was born in Portugal in 1970. In 1993, he became researcher in the Center of Excellence for Microelectronics and Optoelectronics Processes-UNINOVA, Lisbon, Portugal. He graduated in Physics and Materials Engineering from the Faculty of Sciences and Technology from the New University of Lisbon in 1995. Currently, he is Assistant Professor in Electronics Department of ISEL, Lisbon, Portugal, and investigator in the group of Applied Research in Microelectronic Optoelectronic and Sensors-GIAMOS in the same institution.

João Martins was born in Lisbon, Portugal, in 1961. He graduated in Electrotechnical and Computer Engineering, branch of Telecommunications and Electronics, from the Technical University of Lisbon (IST) in 1988. In 1993, he received the Master of Science in Electrotechnical and Computer Engineering from the Technical University of Lisbon. In 1987, he became researcher member of the Microelectronics Group of the Systems and Computers Engineering Institute (INESC), Lisbon. In 1996, he became Professor of Semiconductors and Microelectronics in ISEL, Lisbon. Currently, he is member of the Group in Applied Research in Microelectronics, Optoelectronics and Sensors, GIAMOS at ISEL in Lisbon, Portugal. J. Martins has several scientific papers and more than 10 years of research and development experience in several fields of interest, mainly related to computer-aided design for electronics, and semiconductor devices and sensors.

Paula Louro Antunes was born in Portugal in 1967. In 1990, she became researcher in EID (a company of research and development in the field of electronics), Lisbon, Portugal, in the Department of Optoelectronics. She graduated in Physics from the Faculty of Sciences from the University of Lisbon in 1990. In 1995, she received the Master of Science in Material Engineering by the New University of Lisbon. Currently, she is Assistant Professor in the Electronics Department of ISEL, Lisbon, Portugal, where she teaches Electronic and Semiconductor Physics. Her main research interest is in the field of amorphous semiconductor thin films.

António Maçarico was born in Evora, Portugal, in 1960. He received his degree in Physic and Materials Engineering from New University of Lisbon in 1988. Between 1983 and 1987, he worked as collaborator in the Molecular Physics Center Line 6 of INIC (National Institute of Scientific Research), Portugal, where the work was devoted to characterisation and production of amorphous silicon. In 1989, he joined PORTSOL (TUDOR group) involved in a project of technology transfer between University and Industry for the industrial production of amorphous solar cells. From 1991 to 1997, he worked as researcher at UNINOVA, Lisbon, Portugal. Currently, he is Adjunct Professor in ISEL, Lisbon, Portugal.

Reinhard Schwarz was born in Großköris, Germany, in 1950. He received the degree in Physics and Mathematics from the University of Stuttgart, Germany, in 1977. He joined the Physics Department in Neuchâtel University, Switzerland, where he was teacher and where he received his PhD in 1982. After that he became scientific collaborator in the Institute of Microtechnology, University of Neuchâtel, Switzerland, until 1983 when he joined the group of Professor S. Wagner in the Department of Electrical Engineering, Princeton University, USA. Later, he joined the Physics Department E16 of Technische Universität München, Germany, until 1996. Since then he teaches as Invited Professor in the Physics Department in Instituto Superior Técnico, Lisbon, Portugal, and Coordinator Professor in Electronics Department of Instituto Superior de Engenharia de Lisboa, Portugal.

Markus B. Schubert was born in Germany in 1958. He got the Diploma in Electrical Engineering (degree Dipl.-Ing.) from the Faculty of Electrical Engineering of the University of Stuttgart in 1985. In the same year, he joined the Institute of Physical Electronics in the University of Stuttgart as a research associate in the amorphous silicon group. The main working topic was materials research for thin film solar cells. In 1992, he received the PhD in Electrical Engineering (degree Dr.-Ing.) from the Faculty of Electrical Engineering of the University of Stuttgart. From 1992 to 1996, he lectured in the University of Ulm (Germany) as Professor of Energy Conversion and Storage. Since 1996, he is group leader in ''Thin Film Sensors'' at Institute of Physical Electronics, Stuttgart University, managing various research programmes on thin film sensors and solar cells. Currently, he is Associate Director of Institute of Physical Electronics at Stuttgart University (Germany).